Materials and Design 198 (2021) 109391

Contents lists available at ScienceDirect

Materials and Design

journal homepage: www.elsevier.com/locate/matdes

Influence of sodium nitrate on the phases formed in the $MgO-Al_2O_3-SiO_2-H_2O$ system

Ellina Bernard [a,b,*], Barbara Lothenbach [a,b], Daniel Rentsch [c]

[a] Empa, Swiss Federal Laboratories for Materials Science and Technology, Laboratory for Concrete & Construction Chemistry, 8600 Dübendorf, Switzerland
[b] University of Bern, Institute of Geological Sciences, Rock water interaction Group, 3012 Bern, Switzerland
[c] Empa, Swiss Federal Laboratories for Materials Science and Technology, Laboratory for Functional Polymers, 8600 Dübendorf, Switzerland

HIGHLIGHTS

- Magnesium alumino silicate hydrate is the main product of the $MgO-Al_2O_3-SiO_2-NaNO_3-H_2O$ system at low Al content (8-16 wt.%)
- Precipitation of hydrotalcite decreases the incorporation of aluminium in the magnesium alumino silicate hydrate
- Possible formation of zeolitic-like precursor (N-A-S-H) gels in low content
- Small uptake of sodium in the diffusive layer of the solids occurs at this pH (~ 8–10)

GRAPHICAL ABSTRACT

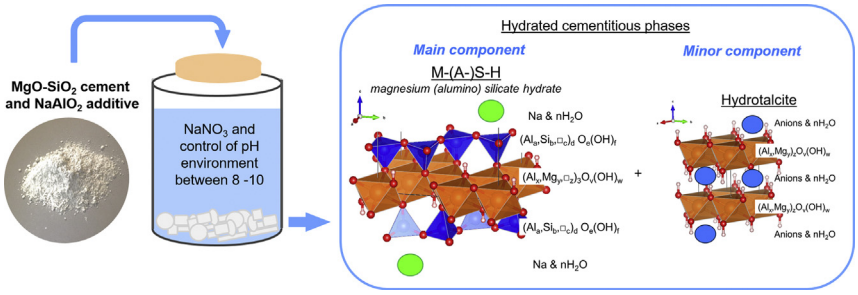

ARTICLE INFO

Article history:
Received 14 May 2020
Received in revised form 4 December 2020
Accepted 4 December 2020
Available online xxxx

Keywords:
Magnesia silicate cement
Alkali magnesia alumino silicate cement
Phase assemblage
Magnesium silicate hydrates M-S-H
Magnesium alumino silicate hydrates M-A-S-H
Hydrotalcite

ABSTRACT

The incorporation of sodium and aluminium in magnesium silicate hydrate phases (M-S-H), possible binding phases in magnesium silicate cement, was investigated. Magnesium alumino silicate hydrate containing sodium (M-A-S-H N samples) were synthesized in batch experiments with $NaNO_3$ ~ 100 mmol/L at Mg/Si ratios equal to 0.8 and 1.2, and Al/Si ratios of 0, 0.1 and 0.2, and equilibrated at 20 and 50 °C. Thermogravimetric analysis (TGA), X-rays diffraction (XRD), ^{29}Si MAS NMR data showed that M-A-S-H phases formed, with a similar structure as M-S-H. ^{27}Al and ^{23} Na MAS NMR data showed that only little sodium was sorbed, while aluminium was possibly incorporated in both tetrahedral and octahedral sites of M-A-S-H. We found evidence that the presence of sodium nitrate led to the formation of hydrotalcite-like phase probably containing NO_3^- and possibly to the trace formation of hydrated alumino-silicate containing sodium: N-A-S-H gel. These minor phases limited the aluminium uptake by M-S-H at higher Al contents (Al/Si = 0.2).

1. Introduction

The manufacture of Portland clinker is an energy intensive process and causes 5 to 8% of the anthropogenic CO_2 emissions. The use of reactive magnesium from magnesium silicate minerals is in consideration to decrease the CO_2 emitted from construction [1]. Thus magnesium silicate hydrate phases get increasing attention as reaction product of magnesium-based binders, a potential alternative to Portland cement [2] and cementitious material able to generate high compressive strength [3,4]. The properties of magnesium silicates hydrate (M-S-H) are also of interest as they are observed at the interfacial zone of cement-based materials in contact with clays [5–9] and/or as secondary products from the degradation of cementitious materials by groundwater or seawater [10–13]. M-S-H is formed from the reaction of magnesium with amorphous silica, released by the decalcification of the

* Corresponding author at: University of Bern, Institute of Geological Sciences, Rock water interaction Group, 3012 Bern, Switzerland.
E-mail address: ellina.bernard@geo.unibe.ch (E. Bernard).

https://doi.org/10.1016/j.matdes.2020.109391

C-S-H on the surface of the hydrated cement. In the case of primary product, M-S-H is formed directly from reactive MgO-SiO_2 sources.

M-S-H phases have an ill-defined structure comparable to hydrated precursors of 2:1 and 1:1 phyllosilicates [8,14–16]. Magnesium phyllosilicates are composed of tetrahedral sheets containing Si^{4+} and octahedral sheets containing Mg^{2+}. One tetrahedral layer on an octahedral layer corresponds to a 1:1 layer silicate structure while two tetrahedral layers sandwiching an octahedral layer correspond to a 2:1 configuration as detailed in Fig. 1.

The observation of M-S-H formed in situ at the surface of hydrated cement indicated that aluminium could be present either in the magnesium silicate phases [6,8,12,18] and/or in a hydrotalcite [5] which is not well crystalline. Our recent study [17] showed the incorporation of aluminium in M-S-H with Mg/Si equal to 1.1 and 1.7 up to Al/Si ~ 0.15–0.18 in synthesized M-S-H phases containing MgO-Al_2O_3-SiO_2-H_2O, together with the possible formation of semi amorphous hydrotalcitic or aluminium hydroxide gels. The uptake of aluminium in M-A-S-H has been observed in both octahedral and tetrahedral layers, similar to phyllosilicates such as vermiculites $(Ca_{0.5}Mg_{0.5}Na\cdot nH_2O)_x\ (Mg,Al,\square)_3[(Al,Si)_4O_{10}](OH)_2\cdot mH_2O$ (where □ is a vacant site). The incorporation of aluminium did not change the main properties of the formed M-A-S-H: a comparable polymerization degree of the tetrahedral silicates with surface charge as M-S-H was observed [17]. At a pH below 10.5 a negative surface charge of M-S-H with a maximum exchangeable cation/Si ~ 0.05 was observed; magnesium, sodium and as well as other cations present have been observed at such cation exchange sites [19]. The potential uptake of sodium by M-A-S-H can modify the pH values and the phase assemblage and the stability at the interface clay-cement [8,9,20] or in new binders [21].

Magnesium in hydrated Portland cement pastes is present as a hydrotalcite-like phase, often intermixed with C-S-H [22–25]. Hydrotalcites have a layered double hydroxides (LDH) structure and variable Mg/Al ratio: $[Mg_{1-x}Al_x(OH)_2]^{x+}\ [A_{x/n}{}^{n-}\cdot mH_2O]^{x-}$, with $0 < x < 0.33$ [26]; "A" indicates the presence of charge compensating anions such as OH^-, Cl^-, NO_3^-, CO_3^{2-}, SO_4^{2-} in the interlayer. The affinity of the compensation anions is $CO_3^{2-} > SO_4^{2-}$ for divalent anions and $OH^- > F^- > Cl^- > Br^- > NO_3^- > I^-$ for monovalent anions [26]. In the presence of high alkali concentrations and of SiO_2 and Al_2O_3, the formation of zeolites or zeolitic precursors may also occur. Zeolite formation is often observed at elevated temperatures (50 °C–70 °C) [27,28], but lower temperatures have also been reported [29–31].

In the present study, M-A-S-H N samples were synthesized with Mg/Si = 0.8 and 1.2 and Al/Si = 0, 0.1 and 0.2 in 100 mmol/L $NaNO_3$ solution. We investigated the stability of M-A-S-H phases at different temperatures (20 and 50 °C) with the addition of sodium nitrate and the possible formation of other phases. The aqueous phases were analysed by ion chromatography and pH measurements and the solid phases by thermogravimetric analysis, X-ray diffraction, ^{29}Si, ^{27}Al and ^{23}Na MAS NMR spectroscopy. The experimental investigations were supported by thermodynamic calculations to better understand the MgO-Al_2O_3-SiO_2-$NaNO_3$-H_2O system.

2. Materials & methods

2.1. Synthesis

In the following the nomenclature M-S-H x, M-S-H xN, M-A-S-H x y, and M-A-S-H xN y is adopted to describe the samples, where x indicates the Mg/Si ratio, y the Al/Si ratio, and N the presence of $NaNO_3$.

Magnesium oxide (Merck, pro analysis, 0.18 ± 0.02 wt% Na_2O, surface area of 24 m^2/g [32]) and silica fume (SiO_2, Aerosil 200, 0.9 wt% HCl, specific surface area of 200 m^2/g) were chosen as starting materials for the synthesis of M-S-H x and M-S-H xN synthesized in presence of sodium nitrate ($NaNO_3$, VWR chemicals, Analar normapur) as detailed in [19,32]. Sodium aluminate ($NaAlO_2$, anhydrous, technical from Sigma Aldrich, which contains 6.9 wt% of water as quantified by TGA) was used to synthetize M-A-S-H xN y samples. To avoid the increase of pH value by the addition of sodium aluminate which usually lead to the slower formation of M-S-H due to preliminary formation of brucite [32] a corresponding amount of nitric acid (HNO_3, Merck, suprapur, 65%) was added. In addition, sodium nitrate was added until a total sodium concentration of 100 mmol/L was reached. Two Mg/Si ratios were studied (0.8 and 1.2) and the Al/Si in the mixtures was 0, 0.1 and 0.2 as indicated in Table 1. The samples were prepared in PE-HD containers using milli-Q water and a water/solid (W/S) ratio of 45 to ensure a homogeneous suspension and sufficient solution for analysis. All sample handling was carried out in a glove box under N_2 to avoid CO_2 contamination. The samples equilibrated at 20 °C were placed on a horizontal shaker (100 rpm) and the samples stored at 50 °C were shaken once per week.

The suspensions were equilibrated at different temperatures (20 and 50 °C) and for different times (up to 1 or 2 years) for kinetic and long-term investigations as mentioned in previous work [32]. The solid and liquid phases were separated by filtration under pressure (4–5 bars N_2) using nylon filters (0.45 μm). After filtration, the solids were washed with 50/50 (v/v) water-ethanol and then with 94 wt% ethanol to remove dissolved ions and to prevent the precipitation of salts during drying [33]. The samples were freeze-dried with liquid nitrogen (for approximatively 20 min at −196 °C) and kept for 7 days at −40 °C under vacuum (pressure of 0.28 mbar). After further equilibration in N_2-filled desiccators at a relative humidity of ~30% (above saturated $CaCl_2$ solution) over a period of at least 14 days, the solid phases

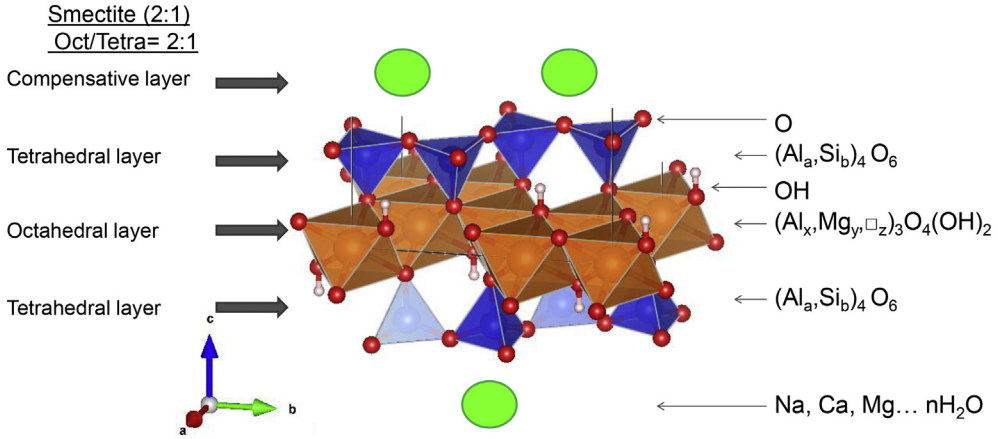

Fig. 1. Schematic sketches of phyllosilicate structure (reproduced from [17]).

Table 1
Starting materials and sample compositions used for the preparation of M-S-H x, M-S-H xN and M-A-S-H xN y samples ($MgO + SiO_2 + NaAlO_2 + NaNO_3 + HNO_3$).

Sample	*M-S-H 0.8*	*M-S-H 0.8 N*	M-A-S-H 0.8 N 0.1	M-A-S-H 0.8 N 0.2	*M-S-H 1.2*	*M-S-H 1.2 N*	M-A-S-H 1.2 N 0.1	M-A-S-H 1.2 N 0.2
$[NaNO_3]$ (mmol/L) [a]	*0*	*~ 100*	~ 100	~ 100	*0*	*~ 100*	~ 100	~ 100
MgO (g)	*1.75*	*1.75*	1.6	1.48	*2.23*	*2.23*	2.07	1.94
SiO_2 (g)	*3.25*	*3.25*	2.99	2.76	*2.77*	*2.77*	2.58	2.41
$NaAlO_2$ (g)	–	–	0.44	0.81	–	–	0.38	0.7
$NaNO_3$ (g)	–	*1.91*	1.56	1.26	–	*1.91*	1.61	1.35
$[HNO_3]$ (mmol/L)[b]	–	–	20	35	–	–	28	48
[Na] (mmol/L) [c]		*100*	105	110		*100*	105	109
$[NO_3]$ (mmol/L) [d]		*100*	102	101		*100*	112	119
H_2O (milliQ water) (g)	*225*	*225*	225	225	*225*	*225*	225	225

Samples from [19,32] which were not prepared in the present work are shown in italic font.
[a] Targeted concentration.
[b] Acid concentration in the 225 g of water.
[c] [Na] = [mass ($NaAlO_2$)/Molar mass($NaAlO_2$) + mass ($NaNO_3$)/Molar mass($NaNO_3$)] /0.225*1000.
[d] $[NO_3]$ = mass ($NaNO_3$)/Molar mass($NaNO_3$)/0.225*1000 + $[HNO_3]$.

were analysed. After drying, the samples were gently ground by hand and then stored again in N_2-filled desiccators at a relative humidity of ~30%. The focus is made on the samples equilibrated 2 years at 20 °C and 1 year at 50 °C.

The M-A-S-H 1.2 N 0.1 and M-A-S-H 1.2 N 0.2 samples will be compared to M-A-S-H 1.1 0.1 from [17] in the results and discussions, as it is a pure M-A-S-H phase without hydrotalcite, brucite, microcrystalline Al $(OH)_3$ or unreacted silica. The ratio of 1.1 is slightly lower compared to 1.2; however, the possible hydrotalcite formation in the M-A-S-H 1.2 N 0.1 and M-A-S-H 1.2 N 0.2 samples as discussed below also decreases the effective Mg/Si in the samples.

For comparison, crystalline hydrotalcite with targeted formula $Mg_6Al_2(NO_3)_2(OH)_{16} \cdot mH_2O$ ($[Mg_{1-x}Al_x(OH)_2]^{x+}$ $[A_{x/n}{}^{n-} \cdot mH_2O]^{x-}$, with $x = 0.25, n = 2$) was synthesized over 20 days at 80 °C from amorphous $3MgO.Al_2O_3$ put in 1.2 M $NaNO_3$ solution prepared from $NaNO_3$ salt (Merck, for analysis, purity >99.5%) with a liquid/solid ratio equal to 10. The solutions were prepared to force the NO_3^- incorporation in the solid. The solid obtained from filtration was washed, dried and then stored as described for the M-A-S-H samples. No liquid analysis was performed for this sample. The XRD data of the solid is presented in Fig. S1 (Supporting Information), TGA and ^{27}Al MAS NMR data are shown in the following for comparison.

2.2. Analytical techniques

The compositions of the liquid phases were analysed by ion chromatography (IC) immediately after filtration. The concentrations of the dissolved magnesium, sodium, nitrate were quantified using a Dionex DP series ICS-3000 ion chromatography system with a measurement error ≤ 10% in undiluted solutions or in solutions diluted by factors of 10, 100 or 1000. Dissolved silicon was analysed using sodium carbonate/bicarbonate eluent and sodium molybdate, and sodium lauryl sulphate in metasulfonic acid as a post-column reagent using an ion pack AS22 column. Dissolved aluminium was analysed using CS5A Dionex IonPac column with HCl diluted eluent with a post column reagent (ammonium acetate).

All concentrations were determined as duplicates and the results are given as mean values. The pH values (±0.1) were measured at ambient temperature (23 ± 2 °C) in an aliquot of the unfiltered suspension and the results were corrected to 20 or 50 °C [32]. The composition of the aqueous phase did not change significantly during the 30 min required to cool the solutions from 50 °C to ambient temperature [32].

XRD data were collected using a PANalytical X'Pert Pro MPD diffractometer equipped with a rotating sample stage in a Θ-2Θ configuration applying CuKα radiation (λ = 1.54 Å) at 45 mV voltage and 40 mA intensity with a fixed divergence slit size and an anti-scattering slit on the incident beam of 0.5° and 1°. All samples were scanned between 5° and 75° 2Θ with a X'Celerator detector.

The ^{29}Si MAS NMR single pulse experiments were conducted on a Bruker Avance III NMR spectrometer using a 7 mm CP/MAS probe at 79.5 MHz applying the following parameters: 4500 Hz sample rotation rate, minimum of 3072 scans, 30° ^{29}Si pulse of 2.5 μs, 20 s recycle delays, RF field strength of 33.3 kHz during SPINAL64 proton decoupling. The ^{29}Si NMR chemical shifts were referenced to the most intense resonance at −2.3 ppm of an external sample of an octamethylsilsesquioxane (Aldrich No. 52,683–5) which was referenced to tetramethylsilane (TMS, $\delta^{29}Si = 0.0$ ppm). For ^{29}Si MAS NMR data, the 30° flip angle is a compromise between improving signal to noise and quantitative data acquisition. With the applied recycle delay of 20 s, this experimental setup yields a maximum signal for species with T_1 recycle times of 120 s according to the Ernst angle. For a representative sample (M-S-H 0.8 N cured at 50 °C during 1 year) we obtained T_1 values in the range of 65 to 80 s applying a ^{29}Si MAS NMR saturation recovery pulse sequence. Although the maximum signal intensity was not reached with the selected flip angle, the magnetisation in the observed window of T_1 values relaxed similarly under these conditions (ca. 90% of equilibrium magnetisation recovered after each pulse). Assuming that the T_1 values do not change between samples, the changes in relative signal intensities obtained by lineshape analysis of the Q^n sites within each sample were evaluated.

The observed ^{29}Si NMR resonances were assigned using the Q^n classification, where one Si tetrahedron is connected to n Si tetrahedra, where n varies from 0 to 4. The lineshapes of the experimental data were analysed by non-linear least-square fits using the "DMFIT" software developed by Massiot et al. [34]. The presence of unreacted silica was confirmed by the resonances at −101 ppm (Q^3 from the surface of the amorphous silica [14]) and of Q^4 at −110 ppm. The procedure used for the lineshape analysis of ^{29}Si NMR data is described in detail in [32].

The ^{27}Al NMR spectra were measured on the same instrument using a 2.5 mm CP/MAS probe. The ^{27}Al MAS NMR single pulse experiments were recorded at 104.3 MHz applying the following parameters: 25′ 000 Hz sample rotation rate, between 2000 and 4000 scans depending on the content of aluminium in the samples, π/12 pulses of 1.5 μs, 0.5 s recycle delays (identical spectra were obtained when recycle delays of 0.2, 0.5 and 1.0 s were applied), without ^{1}H decoupling. The ^{27}Al NMR chemical shifts were referenced to an external sample of Al $(acac)_3$. The ^{27}Al MAS NMR spectra were analysed by the above mentioned lineshape fitting software "DMFIT" [34]. The detailed description of the lineshape fitting procedure is given in the Supporting Information section.

The ^{23}Na MAS NMR data was recorded at 105.9 MHz using a 4 mm CP/MAS probe applying the following parameters: 13′000 Hz sample rotation, 512 scans, 20° pulses of 2.0 μs, 1 s recycle delays, no ^{1}H decoupling during acquisition. The ^{23}Na chemical shifts were externally referenced to a 0.1 M solution of NaCl in D_2O [35] and the lineshapes

were analysed by applying Lorentzian lineshapes [34]. Please note that the ^{23} Na MAS NMR resonances throughout were symmetrical and lineshapes could be simulated by using Lorentzian shapes. All attempts to fit the ^{23}Na NMR data with 2nd order quadrupolar broadened lineshapes failed, which means that the sodium cations must be quite mobile in the M-S-H N phases.

To obtain uniformly excited NMR resonances, small flip angels of 20 and 8° were applied to record ^{23}Na and ^{27}Al MAS NMR data, respectively [36]. The recycle delays applied ensure the recording of quantitative data.

2.3. Saturation indices

The calculations of the saturation indices were carried out using the Gibbs free energy minimization program GEMS [37]. GEMS is a broad-purpose geochemical modelling code which computes equilibrium phase assemblage and speciation in a complex chemical system from its total bulk elemental composition. The thermodynamic data for aqueous species and for brucite ($Mg(OH)_2$) were taken from the GEMS version of the PSI/Nagra thermodynamic database [38]. The data for the M-S-H solid solution and for amorphous SiO_2 originate from [32,39] and M-A-S-H phases added to the solid-solution from [17], for microcrystalline aluminium hydroxide (microcrystalline Al$(OH)_3$) from [40,41], hydrotalcite from [42], and the zeolite phases from [43] as summarized in Table 2.

The saturation indices (SI) of the different solids were calculated based on the experimentally determined ion concentrations in solution according to eq. (1):

$$SI = \log \frac{IAP}{Kso} \quad (1)$$

where IAP is the ion activity product calculated from the measured concentrations, while Kso is the theoretical solubility product of the solid (as indicated in Table 2).

3. Results and discussions

3.1. TGA and XRD data

The TGA data of the M-A-S-H xN y samples synthesized at 20 and 50 °C are shown in Fig. 2a-d. For comparisons reasons, available data of M-S-H x [32], M-S-H xN [19] and M-A-S-H y [17] are presented in Fig. 2. In addition, TGA of hydrotalcite, aluminium hydroxide and brucite from [44], of synthesized NO_3-hydrotalcite are additionally included in Fig. 2e. XRD patterns of the M-A-S-H xN y samples with the M-S-H xN samples, cured at 20 °C and 50 °C, respectively, are shown in Fig. 3.

The XRD and TGA data (Fig. 2 and Fig. 3) show strong similarities between the M-S-H x or M-S-H xN and the M-A-S-H xN 0.1 samples. The broad humps at 19.7, 26.7, 35.0, and 59.9°2θ (λ = 1.54Å) [14,15] in the XRD data of the M-A-S-H xN y samples can be assigned to M-S-H (Fig. 3, Table 3). Additionally, the characteristic water losses between 30 and 250 °C (poorly bound water) and 250 °C and 800 °C (chemically bound water: hydroxyl groups) [3,14,45,46] of M-S-H were found (Fig. 2a-d).

For the M-A-S-H xN y samples prepared at 20 °C, the formation of brucite (Fig. 2a, b: water loss centered at ~400 °C [3] and Fig. 3a, b, reflection peaks at 18.6, 32.7, 38.0, 50.9, 58.7, 62.0°2θ [47,48]) was observed. In addition, a poorly crystalline hydrotalcite-like phase (reflection peaks at 11.39, 23.02, 61.35°2θ [49] associated with water loss at 200 and 350 °C [44,49,50]) was identified in the M-A-S-H xN 0.2 samples cured at 20 °C and at 50 °C. Some poorly crystalline hydrotalcite-like phases and/or amorphous aluminium hydroxide may also have formed in M-A-S-H xN 0.1, but in small amounts difficult to identify by TGA and XRD. Finally, the presence of semi crystalline or even amorphous aluminium hydroxide (water loss at ~100 °C (amorphous) or 250–300 °C (semi-crystalline) [44,51]) is possibly observed in samples that were aged at all temperatures. All the solids detected are summarized in Table 3.

Comparing the samples equilibrated for 1 year at 50 °C, i.e. the samples which were in equilibrium as discussed in [32], the M-A-S-H xN 0.2 samples showed clearly the presence of a hydrotalcite-like phase, which is present only in trace amounts in M-A-S-H 1.1 0.2 sample [17], indicating tentatively an important role of sodium nitrate in hydrotalcite formation.

Finally, for M-A-S-H xN 0.2 samples some additional broad humps in XRD can be observed at ~14, 28 and 44°2θ, which could not be associated with any of the above discussed solid phases. There are two possible explanations for these reflections: the presence of amorphous aluminium hydroxide with broad humps in XRD data at ~14, 29, 39 and 49°2θ, usually attributed to amorphous aluminium hydroxide/boehmite [52]; or the formation of hydrated alumino-silicate containing sodium (N-A-S-H gels) as precursors of zeolites that could present pattern with broad reflections assigned to e.g. sodalite 14.1, 24.6, 35.0, 43.2°2θ [53] or zeolite Y(Na) 6.2, 10.1, 11.9, 15.6, 20.3°2θ [54].

3.2. NMR data

^{29}Si MAS NMR data (Fig. 4) confirm the presence of M-S-H in all M-A-S-H xN y samples; about 2/3 of the signal intensity is attributable to Q^3 species between −93 and − 97 ppm and approximately 1/3 to Q^2 at −85 ppm [14,55–59]. The results from lineshape analysis (see experimental part) for M-A-S-H xN y samples are presented in Table 4. At 20 °C, all samples excepted M-A-S-H 1.2 N 0.1 sample showed

Table 2
Standard thermodynamic properties (25 °C) and molar volumes of the phases considered in this study with indication of references.

		logK$_{so}$[a]	$\Delta_f G°$ (Gibbs free energy of formation)	V° (molar volume)	
			[kJ/mol]	[cm^3/mol]	Ref.
M-S-H solid solution					
Mg/Si = 0.78	$(MgO)_{0.78}(SiO_2)_1(H_2O)_{1.48}$	−14.59	−1682.18	57	[32]
Mg/Si = 1.30	$(MgO)_{1.30}(SiO_2)_1(H_2O)_{1.80}$	−21.44	−2073.47	71	[32]
Mg/Si = 0.75	$(MgO)_{0.75}(Al_2O_3)_{0.1}(SiO_2)_1(H_2O)_{2.15}$	−15.0	−1985.24	58	[17]
Mg/Si = 1.50	$(MgO)_{1.50}(Al_2O_3)_{0.1}(SiO_2)_1(H_2O)_{3.32}$	−24.0	−2684.16	75	[17]
Brucite	$Mg(OH)_2$	−11.16	−832.23	24.6	[38]
OH-hydrotalcite 2:1	$Mg_4Al_2(OH)_{14}(H_2O)_3$	−56.0	−6394.6	22	[42]
Microcrys. Al$(OH)_3$	$Al(OH)_3$	−0.67	−1265.28	31.95	[40]
$SiO_{2,amorphous}$	SiO_2	−2.9	−849.96	29	[32]
Sodalite	$Na_8Al_6Si_6O_{24}(OH)_2 \cdot 2H_2O$	−65.2	−1322.15	425	[43]
Natrolite	$Na_2Al_2Si_3O_{10} \cdot 2H_2O$	−26.6	−5305.15	169	[43]
Zeolite X(Na)	$Na_2Al_2Si_{2.5}O_9 \cdot 6.2H_2O$	−21.9	−5857.79	196	[43]
Zeolite Y(Na)	$Na_2Al_2Si_4O_{12} \cdot 8H_2O$	−29.5	−7578.22	283	[43]

[a] All solubility products refer to the solubility with respect to the aqueous species Na^+, Mg^{2+}, AlO_2^-, SiO_2^0, OH^-, or H_2O.

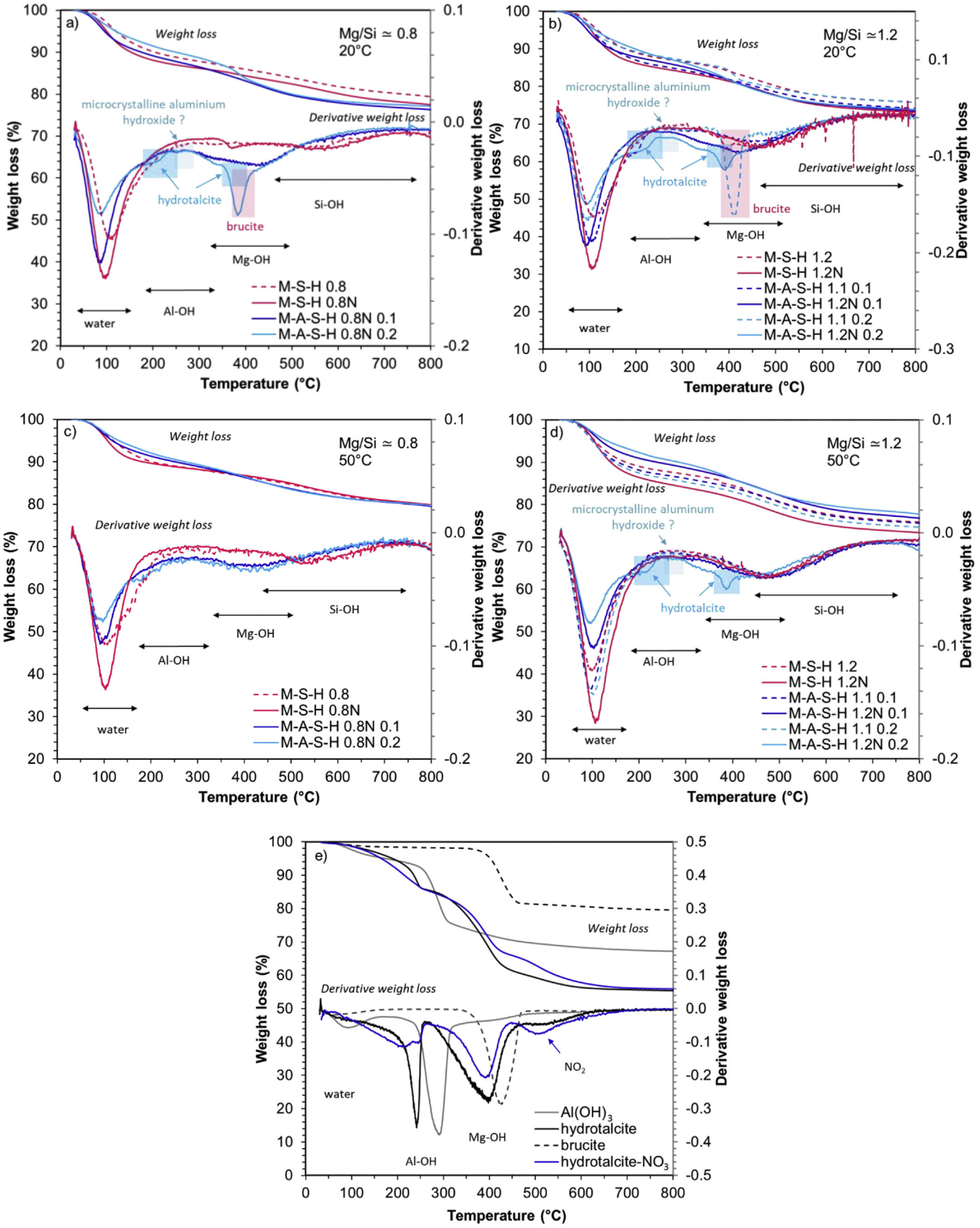

Fig. 2. Thermogravimetric analyses of M-S-H x, M-S-H xN, M-A-S-H x y, and M-A-S-H xN y samples incubated for 2 years at 20 °C (a and b) or 1 year at 50 °C (c and d) and of reference materials aluminium hydroxide, hydrotalcite (Mg/Al = 2) and brucite (e); data for samples M-S-H x and M-S-H xN (pink lines) are from [19,32]. (For interpretation of the references to colour in this figure legend, the reader is referred to the web version of this article.)

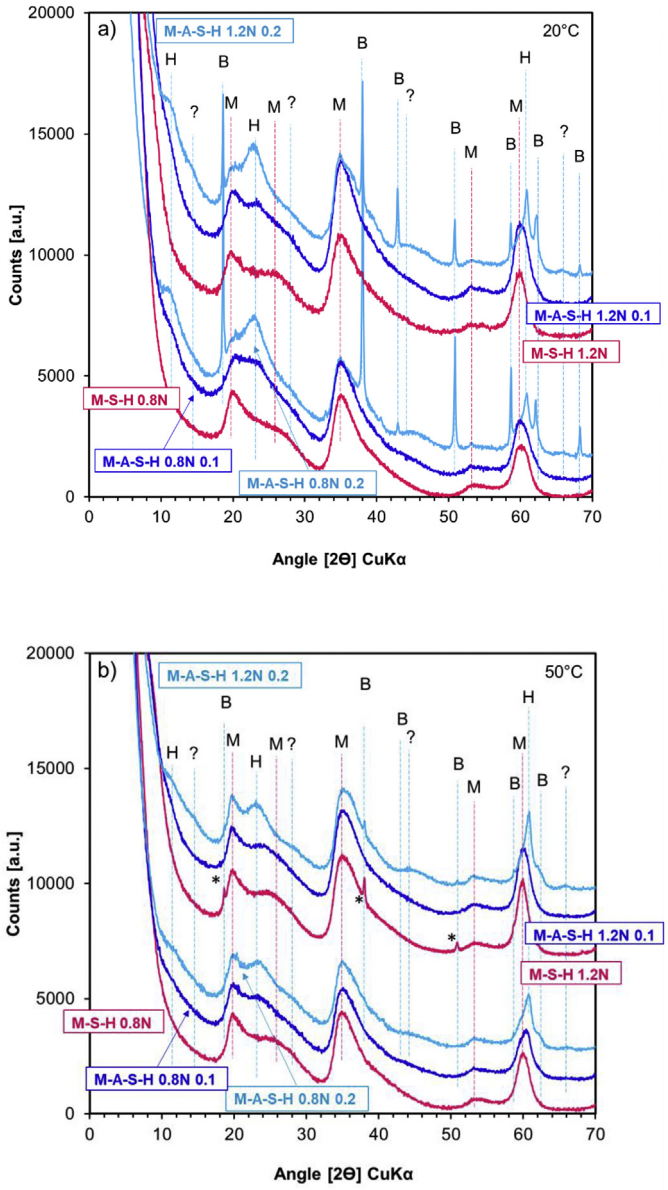

Fig. 3. X-ray diffraction patterns of the indicated samples incubated at (a) 20 °C for 2 years or (b) 50 °C for 1 year (except for M-S-H 1.2 N, which was incubated for 3 months and did not reach equilibrium as indicated by signals of residual brucite marked with asterisks). B = brucite, H = hydrotalcite, M = M-S-H,? = not identified phase. Diffractograms of samples M-S-H x and M-S-H xN are from [19,32].

low-intensity and poorly resolved signals assigned to Q^4 at −110 ppm and Q^3 (OH) at −101 ppm indicating the presence of unreacted amorphous silica. At 50 °C only for M-A-S-H 0.8 N y samples, unreacted silica was identified as observed for M-S-H 0.8 [32], while the M-A-S-H 1.2 N y samples were virtually free of unreacted silica.

In a first step, ^{29}Si MAS NMR data of M-A-S-H samples from [17] were analysed. Acceptable deconvolutions were obtained only when resonances at ca. -82 and − 90 ppm were used in addition to those employed for M-S-H samples (example of deconvolution is given in Fig. S2). Both slightly high frequency shifted ^{29}Si NMR resonances are related to the presence of aluminium next to silica in M-A-S-H phase: Q^2(Al) and Q^3(Al) [17]. The lineshape of M-A-S-H 0.1 0.1 samples cured at 20 and 50 °C (free of sodium and therefore of zeolitic precursor) showed characteristic M-A-S-H signals: Q^1 at −78.5 ppm, Q^2(Al) at −81.7 ppm, Q^2 at −85.6 ppm, Q^3(Al) at −90.4 ppm, Q^3a at −92.9 ppm, Q^3b at −95 ppm, Q^3c at −97 ppm. The M-A-S-H 1.1 0.1 samples cured at 20 and 50 °C showed a Q^2/Q^3 ratio of 0.6–0.7, indicating a slightly higher polymerization degree than in M-S-H where a ratio of about 0.9 is expected [32].

For M-A-S-H xN y samples, reasonable deconvolutions were also obtained with similar signals. However, main ^{29}Si MAS NMR resonances of zeolites such as natrolite usually are also observed between −85 and − 100 ppm, at −87.6 and − 95.2 ppm [60] or for zeolite Y, zeolite X or sodalite at −85, −89 and − 94 and − 100 ppm [61]. Therefore, the unambiguous identification of zeolitic precursors in presence of M-A-S-H phases could be prevented, because their signals would be expected at the same chemical shift region and, furthermore, due to the low crystallinity, rather broad signals would be expected for zeolitic material.

The M-A-S-H 0.8 N y and the M-A-S-H 1.2 N 0.2 samples at 50 °C presented a Q^2/Q^3 ratio about 0.4–0.5, i.e. high Q^3 content, which could be explained either by an effective low Mg/Si in the M-A-S-H phases [32] or by the presence of zeolitic-like type precursors. While the M-A-S-H 1.2 N 0.1 (at 20 and 50 °C) samples and the sample M-A-S-H 1.2 N 0.2 at 20 °C could be free of zeolitic precursors as they showed a Q^2/Q^3 ratio of 0.6–0.7 similar to the pure M-A-S-H 1.1 samples, known as free of zeolitic precursor.

The ^{27}Al MAS NMR spectra of the M-A-S-H xN y samples are shown in Fig. 5 together with the spectrum of a M-A-S-H 1.1 0.1 sample prepared in absence of sodium nitrate [17]. The ^{27}Al MAS NMR spectra of the M-A-S-H xN y samples were simulated based on the deconvolution of M-A-S-H 1.1 0.1 sample discussed in [17] with two or three instead of only one signal with an asymmetric lineshape for the tetrahedral (Al(IV)) sites and two sites Al(*VI*)a and Al(*VI*)b for the octahedral environment (see Supporting Information). In Fig. S3 an example of the deconvolution of a ^{27}Al MAS NMR spectrum (M-A-S-H 1.2 N 0.2) is shown and the results for all M-A-S-H xN y samples are summarized in Table 5. Deconvolution was mainly performed to determine the isotropic ^{27}Al NMR chemical shifts of the species Al(*IV*)a, b, c, but the relative amounts shown in Table 5 are associated with errors of about 10–20%.

For the M-A-S-H 1.1 0.1 sample, only one signal Al(*IV*)b with δ_{iso} of 69 ppm was necessary to fit the chemical shift range of tetrahedrally coordinated Al of the spectra [17]. For most of the M-A-S-H xN y samples (Fig. 5, Fig. S3 and Table 5) three peaks with isotropic chemical shifts of ≈ 80, 68 and 60 ppm were used for the Al(IV) signal, ascribed to three Al(IV) species in different environments named Al(*IV*)a, Al(*IV*)b, and Al(*IV*)c. The isotropic chemical shift at ≈ 80 ppm was attributed to the presence of hydrotalcite which exhibits a minor amount of dehydroxylated Al(VI) (Fig. 5 and [62]). An intensity >5% is observed in samples, where hydrotalcite was confirmed by TGA and XRD.

The Al(*IV*)b peak is attributed to Al(IV) sites in the M-A-S-H phase. The Al(*IV*)c signal is characteristic for zeolites [63,64], however it was not readily observed in each sample, particularly in the samples M-A-S-H 1.2 N 0.1 (cured at 20 and 50 °C) and in sample M-A-S-H 1.2 N 0.2 (cured at 20 °C). For these ^{27}Al NMR spectra deconvolutions were performed without the Al(*IV*)c site. Although the presence of zeolite precursor in our data could not be unambiguously confirmed by XRD or TGA, the ^{27}Al NMR data indicated that poorly crystalline zeolitic precursor may be present in all the M-A-S-H 0.8 N y samples and the M-A-S-H 1.2 N 0.2 at 50 °C.

An average proportion of ~20% for the asymmetric environment Al(*VI*)a at 10–11 ppm was determined for all M-A-S-H xN y samples (Table 5), which corresponds very well to the content of Al(*VI*)a in M-A-S-H samples [17]. Alternatively, the asymmetric Al(*VI*)a resonance may also indicate the presence of poorly ordered aluminium hydroxide gels [65].

Since the ^{27}Al NMR chemical shifts of the Al(*VI*)b sites in M-A-S-H phase and in hydrotalcite are very similar, as in both cases aluminium is completely neighboured by magnesium in an octahedral layer (trioctahedral phyllosilicates or LDH, where all octahedral positions are filled [66] as discussed in detail in [17]), the distinction by ^{27}Al NMR of the two phases is not possible. However, the Al(VI) fraction in

Table 3
Identification of hydrotalcite, brucite, amorphous aluminium hydroxide, unreacted silica, and zeolite precursor in the indicated samples.

Sample	Incubation conditions	Hydrotalcite	$Mg(OH)_2$	Microcrystalline $Al(OH)_3$	Unreacted silica	Zeolitic-precusor
M-S-H 0.8 N	20 °C - 1 year				✓ Si MAS NMR	
M-A-S-H 0.8 N 0.1	20 °C - 1 year	trace? TGA trace XRD ✓? Al MAS NMR	trace? TGA ✓ XRD	trace? TGA ✓? Al MAS NMR ✓? XRD	✓ Si MAS NMR	✓? Si MAS NMR ✓ Al MAS NMR ✓? XRD
M-A-S-H 0.8 N 0.1	20 °C - 2 years	trace? TGA trace XRD ✓? Al MAS NMR	trace? TGA ✓ trace XRD	trace? TGA ✓? Al MAS NMR ✓? XRD	✓ Si MAS NMR	✓? XRD ✓? Si MAS NMR ✓ Al MAS NMR ✓? XRD
M-A-S-H 0.8 N 0.2	20 °C - 1 year	✓ TGA ✓ XRD ✓? Al MAS NMR	trace? TGA ✓ XRD	trace? TGA ✓? Al MAS NMR ✓? XRD	✓ Si MAS NMR	✓? Si MAS NMR ✓ Al MAS NMR ✓? XRD
M-A-S-H 0.8 N 0.2	20 °C - 2 years	✓ TGA ✓ XRD ✓? Al MAS NMR	trace? TGA ✓ trace XRD	trace? TGA ✓? Al MAS NMR ✓? XRD	✓ Si MAS NMR	✓? XRD ✓? Si MAS NMR ✓ Al MAS NMR ✓? XRD
M-S-H 1.2 N	20 °C - 1 year					
M-A-S-H 1.2 N 0.1	20 °C - 1 year	trace? TGA ✓ XRD ✓? Al MAS NMR	✓ TGA ✓ XRD	trace? TGA ✓? Al MAS NMR ✓? XRD		
M-A-S-H 1.2 N 0.1	20 °C - 2 years	trace? TGA ✓ XRD ✓? Al MAS NMR		trace? TGA ✓? Al MAS NMR ✓? XRD		
M-A-S-H 1.2 N 0.2	20 °C - 1 year	✓ TGA ✓ XRD ✓? Al MAS NMR	✓ TGA ✓ XRD	trace? TGA ✓? Al MAS NMR ✓? XRD	✓ Si MAS NMR	✓? XRD
M-A-S-H 1.2 N 0.2	20 °C - 2 years	✓ TGA ✓ XRD ✓? Al MAS NMR	✓ TGA ✓ XRD	trace? TGA ✓? Al MAS NMR ✓? XRD	✓ Si MAS NMR	✓? XRD
M-S-H 0.8 N	50 °C – 1 year				✓ Si MAS NMR	
M-A-S-H 0.8 N 0.1	50 °C – 1 year	trace? XRD ✓? Al MAS NMR		✓? XRD	✓ Si MAS NMR	✓? Si MAS NMR ✓ Al MAS NMR
M-A-S-H 0.8 N 0.2	50 °C – 1 year	✓ XRD ✓? Al MAS NMR		✓? XRD	✓ Si MAS NMR	✓? XRD ✓? Si MAS NMR ✓ Al MAS NMR
M-S-H 1.2 N	50 °C – 1 year					
M-A-S-H 1.2 N 0.1	50 °C – 1 year	✓? Al MAS NMR				
M-A-S-H 1.2 N 0.2	50 °C – 1 year	✓ XRD ✓? Al MAS NMR	trace? TGA trace XRD	trace? TGA ✓? XRD		✓? XRD ✓? Si MAS NMR ✓ Al MAS NMR

the M-A-S-H xN y samples appeared to have a more symmetric and narrower lineshape than obtained for M-A-S-H phase, indicating tentatively the presence of hydrotalcite.

The presence of hydrotalcite in the M-A-S-H xN y samples should also explain the lower Al(IV)/Al(VI) ratio (Table 5) in the samples compared to the M-A-S-H phases [17].

The ^{23} Na MAS NMR spectra of M-A-S-H xN y samples at 50 °C are presented in Fig. 6 together with the spectrum of M-S-H 0.8 N samples and M-S-H 0.8 N* (synthesized in NaOH solution at equilibrium with a pH of 12.5 [19]). The ^{23} Na NMR resonances of all M-A-S-H xN y samples showed symmetrical signals with line widths of 700 ± 50 Hz (Lorentzian shapes determined by "DMFIT" [34], data not shown) at a

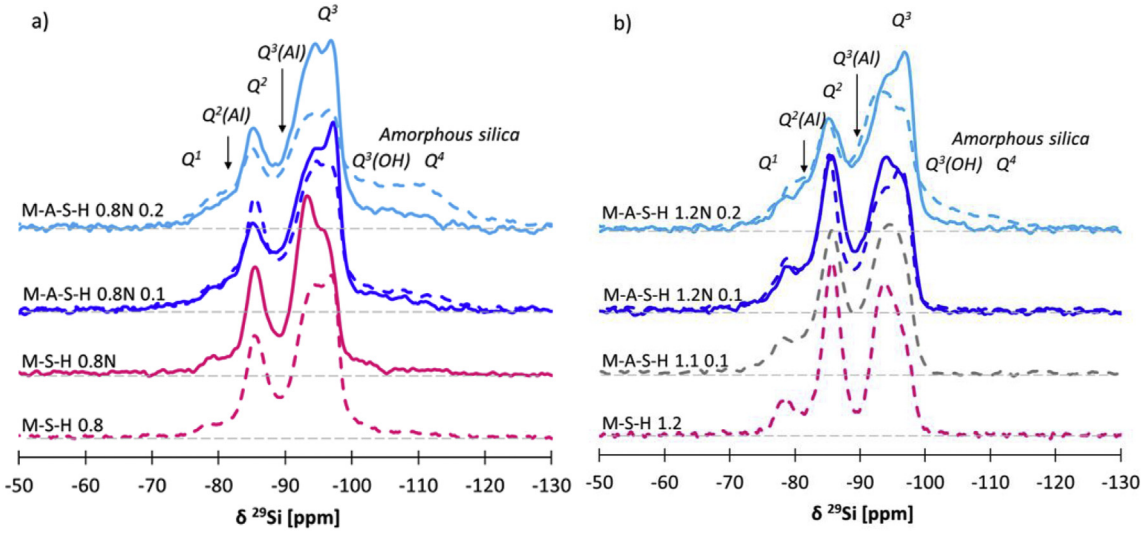

Fig. 4. ^{29}Si MAS NMR spectra with assignments of Q^n environments of the M-A-S-H xN y samples (dark blue lines: y = 0.1; light blue lines: y = 0.2), a) M-A-S-H 0.8 N y samples compared to pure M-S-H 0.8 (pink dotted line) from [32], M-S-H 0.8 N(pink plain line) from [19] b) M-A-S-H 1.2 N y samples compared to pure M-S-H 1.2 (pink dotted line) from [32], M-A-S-H 1.1 0.1 (grey dotted lines) from [17] (plain lines: samples cured at 50 °C, 1 year; dashed lines: samples cured at 20 °C, 2 years). (For interpretation of the references to colour in this figure legend, the reader is referred to the web version of this article.)

Table 4
Assignments of ^{29}Si NMR chemical shifts and relative amounts of Q^n silicon species obtained by simulation of the ^{29}Si MAS NMR spectra shown in Fig. 4.

		Q^1		Q^2(Al)		Q^2		Q^3(Al)		Q^3a		Q^3b		Q^3c		Q^3 (OH)	Q^4	total Q^2	total Q^3	Q^2/Q^3	total silica
	Sample	ppm	[%]	ppm	[%]	ppm	[%]	ppm	[%]	ppm	[%]	ppm	[%]	ppm	[%]	−101	−110				
M-A-S-H																					
20 °C/2 years [17]	M-A-S-H 1.1 0.1	−78.6	6	−81.5	2	−85.6	34	−90.5	8	−92.9	17	−95.0	27	−97.0	5			37	57	0.6	
50 °C/1 year [17]	M-A-S-H 1.1 0.1	−78.3	7	−81.9	4	−85.7	34	−90.4	9	−92.9	16	−95.0	21	−97.0	10			38	55	0.7	
M-A-S-H N																					
20 °C / 2 years	M-A-S-H 0.8 N 0.1	−78.2	3	−80.7	4	−85.4	24	−90.2	8	−92.9	14	−95.2	19	−97.3	12	9	9	28	53	0.5	18
	M-A-S-H 0.8 N 0.2	−78.2	4	−81.9	6	−85.4	14	−90.5	10	−92.9	11	−95.2	10	−97.3	9	14	23	20	40	0.5	37
	M-A-S-H 1.2 N 0.1	−78.6	11	−81.7	5	−85.3	31	−90.0	6	−92.9	17	−95.0	16	−96.9	14			36	53	0.7	
	M-A-S-H 1.2 N 0.2	−78.6	6	−81.5	7	−85.2	23	−90.4	14	−92.9	16	−95.0	10	−97.0	13	7	5	29	53	0.6	12
50 °C / 1 year	M-A-S-H 0.8 N 0.1	−78.2	3	−81.5	4	−85.4	19	−90.2	11	−92.9	17	−95.2	21	−97.3	16	7	3	23	65	0.4	10
	M-A-S-H 0.8 N 0.2	−78.2	2	−81.2	3	−85.4	20	−90.3	12	−92.9	17	−95.2	23	−97.3	13	7	3	23	65	0.4	10
	M-A-S-H 1.2 N 0.1	−78.6	8	−81.8	4	−85.6	35	−90.2	7	−92.9	18	−95.0	17	−97.0	12			39	53	0.7	
	M-A-S-H 1.2 N 0.2	−78.2	5	−81.9	7	−85.4	23	−89.9	12	−92.9	16	−95.2	20	−97.3	17			30	65	0.5	

narrow chemical shift range of – 5.7 ± 1.0 ppm. The observation of signals for the M-A-S-H xN y samples indicated that sodium is present in the solids.

In M-S-H N samples without aluminium incorporation, cation exchange capacity measurements showed poorly sorbed hydrated sodium at the surface of M-S-H [19]. The ^{23}Na NMR resonances of M-S-H 0.8 N and M-S-H 0.8 N* samples showed similar isotropic chemical shifts and line widths (relatively narrow and symmetric signals) as those of M-A-S-H xN y spectra. Therefore, it seems likely that the signals obtained for M-A-S-H xN y samples can be assigned to partially hydrated sodium ($Na(H_2O)_x^+$) at the surface sites on the surface of M-A-S-H. But, the observed chemical shift of the broad ^{23} Na MAS NMR signal between −10 - 0 ppm corresponds also to the expected range of partially hydrated sodium ($Na(H_2O)_x^+$) at the surface sites of N-A-S-H gels [67–71].

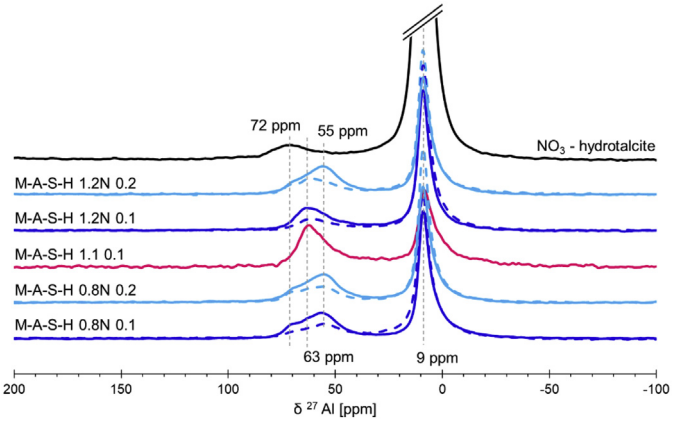

Fig. 5. ^{27} Al MAS NMR spectra of the M-A-S-H xN y samples compared to the M-A-S-H 1.1 0.1 from [17] (plain lines: samples cured at 50 °C, 1 year; dashed lines: samples cured at 20 °C, 2 years) and ^{27}Al NMR spectrum of NO_3-hydrotalcite (black line). The centers of gravity of specific regions are highlighted by dotted lines: The signal at 72 ppm has been assigned to dehydroxylated Al(*IV*)a in hydrotalcite, 63 ppm to Al(*IV*)b in M-A-S-H, 55 ppm to Al(*IV*)c of zeolitic precursor and the Al(*VI*)a and Al(*VI*)b sites at 9–11 ppm to both, M-A-S-H and hydrotalcite. Please note that mean isotropic ^{27}Al NMR chemical shifts of 80, 68 and 60 ppm were determined for the 3 Al(IV) species (Table 5).

Therefore, our data cannot indicate the presence of zeolitic precursor, but indicated only the incorporation of some sodium in the solid phase by sorption of poorly hydrated sodium on the deprotonated silanol groups of M-A-S-H and/or of zeolitic precursor.

All the solids detected by TGA, XRD, and NMR data are summarized in Table 3.

3.3. Analysis of liquid phase

The composition of the liquid phases was also analysed. At 20 °C, a pH of 8.5 was measured in the solution in equilibrium with M-S-H 0.8 sample after 2 years [19] and 0.33 mmol/L magnesium and 1.33 mmol/L silicon. For the M-S-H 1.2 sample, pH increased to 9.9, magnesium decreased to 0.19 mmol/L and silicon to 0.006 mmol/L [19] as indicated in Table 6. In a previous study [17] we showed that the addition of aluminium only to M-S-H did not significantly change the composition of the pore solution. For M-A-S-H 1.1 0.1 sample, pH values remained at about 9.8–10.0 while the silicon concentration remained below 0.01 mmol/L and the magnesium concentrations between 0.1 and 0.4 mmol/L.

Here, the presence of ~100 mmol/L sodium nitrate in the initial solution lowered the pH of M-S-H 0.8 from 8.5 to 7.7 for M-S-H 0.8 N and from 10.3 for M-S-H 1.2 to 9.7 for M-S-H 1.2 N (Table 6). The lower pH and the partial substitution of magnesium by sodium at surface cation exchange sites led to the observed relatively high magnesium concentrations in the presence of sodium nitrate [19]. The pH values of the samples containing sodium and aluminium decrease with time (Table 6). This pH decrease could indicate an uptake of sodium on M-S-H (or zeolitic precursors), in agreement with the observations for M-S-H in absence of aluminium [19].

The solutions of the M-S-H 0.8, M-S-H 0.8 N and M-A-S-H 0.8 N y samples contained silicon concentrations between 1.2 and 1.7 mmol/L indicating equilibria with amorphous silica [14,32]. We observed no influence on magnesium concentrations in samples with low aluminium content (Al/Si = 0.1). However, at Al/Si = 0.2 much lower magnesium concentrations were detected, related to the formation of a hydrotalcite like phase in these samples [17], while silicon concentrations were increased, consistent with the presence of amorphous silica (Table 6). Most concentrations of aluminium were below the detection limit,

Table 5
Compositions and isotropic ^{27}Al NMR chemical shifts of Al (IV) and Al(VI) sites determined by deconvolution of ^{27}Al MAS NMR spectra from M-A-S-H 1.1 0.1 and M-A-S-H xN y samples. Quadrupolar parameters are given in the Supporting Information.

		Al(*IV*)a		Al(*IV*)b		Al(*IV*)c		Al(*VI*)a		Al(*VI*)b		Al(IV)/ Al(VI)
		hydrotalcite		*M-A-S-H*		*Zeolitic precursor*		*M-A-S-H/ Al(OH)$_3$*		*M-A-S-H/ hydrotalcite*		
		δiso	Rel. amount	δiso	Rel. amount	δiso	Rel. amount	δiso	Rel. amount	δiso	Rel. amount	
	Sample	[ppm]	[%]	[ppm]	[%]	[ppm]	[%]	[ppm]	[%]	[ppm]	[%]	
hydrotalcite		80.3	4					10.4	9	9.1	86	0.04
M-A-S-H no Na												
20 °C/2 years [17]	M-A-S-H 1.1 0.1			69.0	38			11.9	22	8.8	40	0.6
50 °C/1 year [17]	M-A-S-H 1.1 0.1			68.8	42			11.6	22	8.4	36	0.7
M-A-S-H N												
20 °C / 2 years	M-A-S-H 0.8 N 0.1	80.3	5	67.8	6	60.4	9	11.2	19	9.2	61	0.3
	M-A-S-H 0.8 N 0.2	80.3	6	67.8	11	60.4	4	11.2	19	9.1	60	0.3
	M-A-S-H 1.2 N 0.1	80.3	2	67.8	12			11.3	21	8.9	65	0.2
	M-A-S-H 1.2 N 0.2	80.3	6	67.8	16			11.3	16	8.9	62	0.3
50 °C / 1 year	M-A-S-H 0.8 N 0.1	80.3	8	68.1	14	60.5	11	11.2	23	9.0	44	0.5
	M-A-S-H 0.8 N 0.2	80.3	9	67.7	15	60.3	13	11.2	15	9.1	48	0.6
	M-A-S-H 1.2 N 0.1	80.3	5	67.6	22			11.3	12	9.0	61	0.4
	M-A-S-H 1.2 N 0.2	80.3	8	67.8	15	60.4	13	11.2	19	9.0	45	0.6

Note: δ_{iso} is the isotropic ^{27}Al NMR chemical shift in the "Czjzek simple" model (see Supporting Information).

indicating a strong preference of Al for the solid phases. No or little reduction of sodium concentrations in the solution was observed, indicating that the sodium uptake by the solid phases observed by ^{23}Na MAS NMR is small only, in accordance with observations for M-S-H samples in the presence of calcium or sodium at low pH [19,72]. Similarly, no specific decrease was observed for the nitrate concentration, indicating only possible little uptake by the solid phase. However, due to the relatively high sodium and nitrate concentrations and their low uptake, such measurements are not very accurate [19,73]. A difference of 10 mmol/L in the measurement corresponds to ~2 mmol of $NaNO_3$ in the solids, a significant amount if related to the Al content in the initial mixes (between 5 and 10 mmol).

As discussed for the experiments performed at 20 °C (see above), similar trends were observed for the samples stored at 50 °C: i.e. highest magnesium concentrations at low Al/Si, decrease of magnesium concentrations with increasing Al/Si and aluminium concentrations at/or below the detection limit.

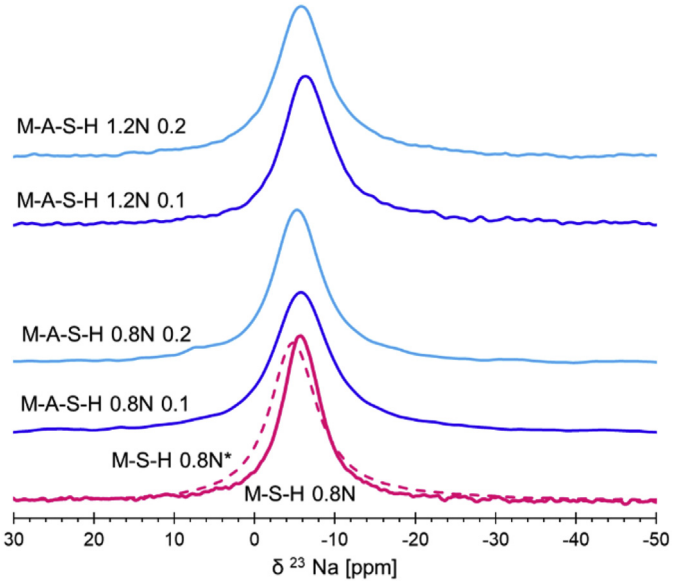

Fig. 6. ^{23} Na MAS NMR spectra of the M-A-S-H xN y samples compared to the M-S-H 0.8 N and M-S-H 0.8 N* (synthesized with NaOH) from [19]; samples cured at 50 °C, 1 year.

3.4. Discussions

Saturation indices were calculated with respect to M-A-S-H, micro crystalline $Al(OH)_3$, OH-hydrotalcite and different zeolites (zeolite X, zeolite Y, natrolite and sodalite, see Table 7); in addition the ion activity products of NO_3-hydrotalcite ($Mg_4Al_2(NO_3)_2(OH)_{12}(H_2O)_3$) and M-A-S-H phases were calculated (see Table 8). Most concentrations of aluminium were below the detection limit, such that in many cases only maximum saturation indices (SI) could be calculated (using the detection limit of 0.0001 mmol/L as maximum aluminium concentration). A negative saturation index (SI) indicates that the solution is undersaturated and the respective solid should not form or will dissolve if present. Thus the knowledge of SI can contribute together with the different solid phase analysis to assess which solids might have formed as discussed for the different solids in the following part.

3.4.1. Hydrotalcite formation

Clear hydrotalcite formation was indicated by TGA for the M-A-S-H xN 0.2 samples, while the XRD and ^{27}Al MAS NMR data tended to indicate the presence of hydrotalcite in all samples containing Al (Table 3).

The SI data (Table 6) indicate that all the samples were undersaturated with respect to OH-hydrotalcite. The formation of OH-hydrotalcite is rather unlikely at pH values <10 (Table 6), i.e. below 0.1 mmol/L hydroxide, while the relatively high nitrate concentration of 100 mmol/L makes the formation of hydrotalcite-containing nitrate instead of hydroxide as counterion in the interlayer probable. Under very similar conditions as in our study, Miyata [26] observed the formation NO_3-hydrotalcite. The measured concentrations indicate an ion activity product of NO_3-hydrotalcite ($Mg_4Al_2(NO_3)_2(OH)_{12}(H_2O)_3$) of 10^{-52} to 10^{-56}, which is in the expected range based on the ion exchange experiments of [26]. In addition, also the presence of some carbonates could stabilise hydrotalcite at pH below 10. The formation of hydrotalcite was also consistent with the significant decrease in magnesium concentration from Al/Si = 0 and 0.1 to Al/Si = 0.2 (Table 6), indicating the precipitation of an Mg and Al containing solid phase. It cannot clearly be assessed whether the nitrate concentrations decreased in the presence of Al, which would indicate uptake into hydrotalcite, owing to the inherent error of the liquid phase analysis of ±10%.

The relatively poor crystallinity of the hydrotalcite-like phases possibly present in the M-A-S-H xN y samples compared to hydrotalcite containing NO_3^- (XRD shown in Fig. S1), is due to its low amount, and the possibility of varying composition both in the interlayer (OH^-, NO_3^-)

Table 6
Measured concentrations of dissolved species, pH values of solutions in equilibrium with the M-A-S-H xN y samples (1 or 2 years of equilibration time at 50 and 20 °C, respectively). Concentrations in mmol/L; errors: pH ±0.1, concentrations: ±10%.

	Incubation conditions	pH (20 °C)	Concentrations					Initially added	
Sample			[Mg]	[Si]	[Al]	[Na]	[NO_3]	[Na]	[NO_3]
M-S-H 0.8	20 °C - 1 year	8.5	0.33	1.36	–	0.33	–	–	–
M-S-H 0.8 N	20 °C - 1 year	7.7	4.27	1.18	–	107	95	100	95
M-A-S-H 0.8 N 0.1	20 °C - 1 year	8.2	3.44	1.36	0.0002	103	111	106	115
M-A-S-H 0.8 N 0.1	20 °C - 2 years	8.1	3.67	1.18	<0.0001	103	102	107	106
M-A-S-H 0.8 N 0.2	20 °C - 1 year	9.1	0.014	1.57	0.009	101	102	111	106
M-A-S-H 0.8 N 0.2	20 °C - 2 years	9.4	0.004	1.71	<0.0001	106	97	113	98
M-S-H 1.2	20 °C - 1 year	10.3	0.10	0.004	–	0.44	–	–	–
M-S-H 1.2 N	20 °C - 1 year	9.7	2.90	0.002	–	99	89	96	99
M-A-S-H 1.2 N 0.1	20 °C - 1 year	10.0	1.59	0.010	<0.0001	104	109	106	118
M-A-S-H 1.2 N 0.1	20 °C - 2 years	8.9	3.84	0.019	<0.0001	106	106	108	109
M-A-S-H 1.2 N 0.2	20 °C - 1 year	9.6	0.006	2.64	<0.0001	120	122	110	125
M-A-S-H 1.2 N 0.2	20 °C - 2 years	9.4	0.006	1.33	<0.0001	123	113	111	117
M-S-H 0.8	50 °C – 1 year	8.1	0.10	2.57	–	0.29	–	–	–
M-S-H 0.8 N	50 °C – 1 year	7.7	2.80	2.53	–	96	106	[a]	[a]
M-A-S-H 0.8 N 0.1	50 °C – 1 year	8.0	1.28	2.04	<0.0001	98	96	[a]	[a]
M-A-S-H 0.8 N 0.2	50 °C – 1 year	8.7	0.04	1.64	<0.0001	107	102	[a]	[a]
M-S-H 1.2	50 °C – 1 year	9.9	0.19	0.006	–	0.50	–	–	–
M-A-S-H 1.2 N 0.1	50 °C – 1 year	8.6	5.07	0.06	<0.0001	104	110	[a]	[a]
M-A-S-H 1.2 N 0.2	50 °C – 1 year	9.1	0.47	0.22	<0.0001	121	118	[a]	[a]

[a] Same solution was used for the samples at 20 and 50 °C.

and the main layer (Mg/Al) which both influence the positions of the XRD signal [74], making both its detection and the exact determination of its composition based on the basal spacing rather inaccurate. The low pH of the solution tentatively indicates the formation of a nitrate containing hydrotalcite-like phase in the M-A-S-H xN y samples, although the presence of nitrate in the hydrotalcite-like phase could not be unambiguously confirmed by XRD.

3.4.2. Are zeolites forming?

The formation of different crystalline zeolites was observed in a similar system containing amorphous SiO_2, $NaAlO_2$, $Mg(OH)_2$ and H_2O, but at higher pH values by Walling et al. [29], while in the present study no crystalline zeolite could be found (see XRD data in Fig. 3). However, the trace formation of poorly crystalline zeolite-like phases (N-A-S-H) seems probable. The ^{29}Si MAS NMR data of the M-A-S-H 0.8 N y samples at each temperature and the M-A-S-H 1.2 N 0.2 at 50 °C sample indicated more Q^3 content than in the other samples (lower Q^2/Q^3), which could indicate the presence of zeolitic precursor in the samples. This high Q^3 content in these samples coincided with the observation of a signal with an isotropic ^{27}Al NMR chemical shift at ~60 ppm in the ^{27}Al MAS NMR data as typical for Al(IV) in zeolite framework.

The solutions were oversaturated with respect to natrolite and zeolite Y (with exception of M-A-S-H 1.2 N 0.1) and close to saturation for sodalite and zeolite X, indicating that the solids could potentially form. However, we want to stress that this is all indirect evidence, which together make the presence of zeolitic precursor probable, while the actual proof of the presence of N-A-S-H gels is difficult; and the exact nature of the zeolitic precursor remains unclear.

3.4.3. Kinetics of M-A-S-H formation

All solutions were nearly saturated with respect to M-S-H and M-A-S-H phases, in agreement with the solid phase analysis, where M-A-S-H phase was identified as the main product. However, the samples synthesized at 20 °C during 2 years show more unreacted silica and brucite than those synthesized at 50 °C during 1 year (Table 3). The samples equilibrated only 1 year at 20 °C exhibit even higher contents of

Table 7
Saturation indices (SI) from measured concentrations (Table 6) and thermodynamic data (Table 2). Experimentally observed solid phases are highlighted in bold.

Sample	Incubation conditions	Saturation indices								
		$Mg(OH)_2$	Microcrystalline $Al(OH)_3$	OH-hydrotalcite[a]	Amorphous silica	MASH[b]	Natrolite	Sodalite	Zeolite X	Zeolite Y
M-S-H 0.8 N	20 °C - 1 year	−5.0			**0.2**					
M-A-S-H 0.8 N 0.1	20 °C - 1 year	**−4.1**	−1.2	***−14.8***	**0.2**	**1.5**	**3.2**	**−9.2**	**−0.2**	**3.4**
M-A-S-H 0.8 N 0.1	20 °C - 2 years	−4.3	−1.3	***−15.8***	**0.2**	**1.0**	**2.5**	**−11.2**	**−0.9**	**2.6**
M-A-S-H 0.8 N 0.2	20 °C - 1 year	**−4.8**	−0.4	***−16.2***	**0.2**	**0.4**	**6.5**	**2.5**	**3.0**	**6.6**
M-A-S-H 0.8 N 0.2	20 °C - 2 years	**−4.7**	−2.6	***−19.9***	**0.1**	**−0.4**	**2.5**	**−8.6**	**−0.9**	**2.6**
M-S-H 1.2 N	20 °C - 1 year	−1.2			−2.9					
M-A-S-H 1.2 N 0.1	20 °C - 1 year	**−0.8**	−2.3	***−4.1***	−2.4	**1.1**	−3.3	−17.3	−5.5	−5.8
M-A-S-H 1.2 N 0.1	20 °C - 2 years	−2.7	−1.2	*−9.2*	−1.7	**−0.5**	−1.2	−15.3	−3.7	−2.9
M-A-S-H 1.2 N 0.2	20 °C - 1 year	**−3.8**	−2.9	***−17.2***	**0.3**	**1.3**	2.6	−8.1	−0.8	2.8
M-A-S-H 1.2 N 0.2	20 °C - 2 years	**−4.2**	−2.5	***−18.0***	**0.0**	**0.2**	2.4	−8.7	−1.0	2.3
M-S-H 0.8 N	50 °C - 1 year	−5.4			**0.5**					
M-A-S-H 0.8 N 0.1	50 °C - 1 year	−5.3	−1.3	*−19.7*	**0.4**	**−0.4**	2.8	−11.6	−0.7	3.2
M-A-S-H 0.8 N 0.2	50 °C - 1 year	−5.7	−1.7	***−22.2***	**0.3**	**−1.7**	2.7	−10.6	−0.8	2.9
M-S-H 1.2 N	50 °C - 1 year									
M-A-S-H 1.2 N 0.1	50 °C - 1 year	−3.7	−0.7	*−12.5*	−1.1	**−1.1**	**0.2**	**−13.9**	**−2.6**	**−1.0**
M-A-S-H 1.2 N 0.2	50 °C - 1 year	−3.9	−1.3	***−14.6***	−0.6	**−0.4**	**1.4**	**−11.2**	**−1.7**	**0.7**

[a] Calculation based on the OH-hydrotalcite from Table 2; the data shown in bold style correspond to the observation of NO_3-hydrotalcite, therefore the values shown in grey style have to be taken with care.
[b] Solid-solution; the data of M-S-H phases from [32] and the M-A-S-H from [17] were considered as indicated in Table 2.

Table 8
Calculated ion activity products (IAP) for M-A-S-H and NO_3-hydrotalcite.

Sample	Incubation conditions	log IAP			
		M-A-S-H			NO_3-Hydro
		Mg/Si = 0.75	Mg/Si = 1	Mg/Si = 1.5	
M-A-S-H 0.8 N 0.1	20°C - 1 year	−14.6	−18.4	−26.0	−52.7
M-A-S-H 0.8 N 0.1	20°C - 2 years	*<−14.8*	*<−18.6*	*<−26.3*	*<−53.5*
M-A-S-H 0.8 N 0.2	20°C - 1 year	−15.0	−19.0	−27.0	−55.9
M-A-S-H 0.8 N 0.2	20°C - 2 years	*<−15.3*	*<−19.3*	*<−27.2*	*<−60.2*
M-A-S-H 1.2 N 0.1	20 °C - 1 year	*<−15.0*	*<−18.0*	*<−24.0*	*<−45.5*
M-A-S-H 1.2 N 0.1	20 °C - 2 years	*<−15.4*	*<−18.8*	*<−25.8*	*<−48.5*
M-A-S-H 1.2 N 0.2	20°C - 1 year	*<−14.7*	*<−18.4*	*<−25.9*	*<−57.9*
M-A-S-H 1.2 N 0.2	20°C - 2 years	*<−15.1*	*<−19.0*	*<−26.7*	*<−58.3*
M-A-S-H 0.8 N 0.1	50°C - 1 year	*<−15.3*	*<−19.4*	*<−27.6*	*<−56.8*
M-A-S-H 0.8 N 0.2	50°C - 1 year	*<−15.8*	*<−20.0*	*<−28.4*	*<−60.5*
M-A-S-H 1.2 N 0.1	50°C - 1 year	*<−15.6*	*<−19.3*	*<−26.7*	*<−50.5*
M-A-S-H 1.2 N 0.2	50°C - 1 year	*<−15.3*	*<−19.1*	*<−26.7*	*<−53.5*

IAP $(M_{0.75}A_{0.1}SH_{1.5}) = \{Mg^{2+}\}^{0.75}\{AlO_2^-\}^{0.2}\{SiO_2^0\}\{OH^-\}^{1.3}\{H_2O\}^{1.5}$;
IAP $(M_1A_{0.1}SH_{1.75}) = \{Mg^{2+}\}\{AlO_2^-\}^{0.2}\{SiO_2^0\}\{OH^-\}^{1.8}\{H2O\}^{1.75}$;
IAP $(M_{1.5}A_{0.1}SH_{1.8}) = \{Mg^{2+}\}^{1.5}\{AlO_2^-\}^{0.2}\{SiO_2^0\}\{OH^-\}^{2.8}\{H2O\}^{1.8}$;
IAP $(Mg_4Al_2(NO_3)_2(OH)_{12}(H_2O)_3) = \{Mg^{2+}\}^4\{AlO_2^-\}^2\{NO_3^-\}^2\{OH^-\}^4\{H2O\}^7$;
{} indicates activity.

amorphous silica and brucite and a higher Al concentration than samples aged of 2 years as shown in Table 3 and Table 6. This indicates that in particular the 20 °C samples are not yet at equilibrium after 1 year in agreement with observation of [3,17]. Increasing the temperature accelerated M-S-H formation and no further changes are observed after 1 year at 50 °C.

The M-S-H formation can be limited by the slow reaction of silica, brucite and $Al(OH)_3$. In general, samples with low Mg/Si may contain unreacted SiO_2 and samples with high Mg/Si may contain unreacted brucite. At high Al/Si levels precipitates of $Al(OH)_3$ can be formed, which are only very slowly incorporated into M-(A-)S-H at 20 °C (increased uptake at 50 °C).

The M-A-S-H 0.8 N y samples were under all conditions oversaturated with respect to amorphous silica in agreement with its presence in the samples as observed by ^{29}Si MAS NMR, the M-A-S-H 1.2 N 0.2 sample only at 20 °C (1 and 2 years), indicating an influence of Al on M-S-H formation rate. All other samples were undersaturated, in agreement with the ^{29}Si MAS NMR data where no unreacted silica was observed (Table 3).

The M-A-S-H 1.2 N 0.2 at 20 °C sample also showed the presence of brucite (Table 3) although the solution was undersaturated with respect to brucite. Brucite formation is generally observed during the early hydration of MgO and SiO_2, as MgO reacts much faster than SiO_2 [3,17]. The dissolution of the formed brucite, however, proceeds only very slowly as it is kinetically hindered in the presence of Si concentrations in the mmol/L range. The presence of both unreacted silica and brucite in this sample (M-A-S-H 1.2 N 0.2 sample) indicates that equilibrium is not yet reached.

The calculated (maximum) SI of microcrystalline $Al(OH)_3$ are all negative indicating undersaturation, which is in agreement with its absence in the solid phase analysis. However, it cannot be excluded that traces could be present which continue to react over time.

3.4.4. Possible incorporations in M-A-S-H

The uptake of Al in both the octahedral and tetrahedral sites of M-S-H in the absence of secondary phases such as hydrotalcite and zeolitic precursors has been evidenced in [17,75]. The formation of hydrotalcite and zeolitic precursors in the present paper due the presence of Na and nitrate led to less Al in M-A-S-H phase than observed for the pure M-A-S-H samples from [17], mainly due to the presence of hydrotalcite as evidenced by the narrow and symmetric ^{27}Al NMR resonance at ~9 ppm (Table 5). The ^{23}Na MAS NMR data showed that a part of sodium is sorbed on silicate surface consistent with Na sorption on M-S-H phase without Al [19], while the data from solution analysis revealed only a small Na uptake at the pH range of 8–10.

The measured concentrations were used to calculate ion activity products (IAP, Table 8) for possible aluminium containing M-S-H end-members resulting in log (IAP) = −14.8 ± 1.3 for $M_{0.75}A_{0.10}SH_{1.50}$, log(IAP) = −18.7 ± 1.9 for $MA_{0.10}SH_{1.75}$, and log (IAP) = −26.5 ± 3.1 for $M_{1.50}A_{0.10}SH_{1.80}$. We use the expression IAP rather than solubility product as we cannot assess whether equilibrium has been reached. These values are in the same order as those of samples produced without sodium nitrate [17], indicating no significant effects of sodium on the solubility of M-A-S-H.

4. Conclusions

The aim of this work was to investigate the effect of sodium and nitrate on the aluminium incorporation into magnesium silicate hydrate phases at pH values between 8 and 10. The ^{29}Si MAS NMR data, thermogravimetric analysis (TGA), and X-ray diffraction (XRD) showed that in all cases M-A-S-H was the main hydrate formed.

Our present study demonstrates that the interplay of sodium, nitrate and aluminium in the presence of magnesium and silicate leads to several different phases: M-A-S-H as the main hydrate, hydrotalcite-like phase possibly containing nitrate and a zeolitic gel phase, which limited the Al-uptake into M-A-S-H compared to systems without sodium nitrate. The ^{23}Na MAS NMR data indicated that minor amounts of hydrated Na^+ is present at cation exchange sites to compensate the negative charge of M-S-H.

Additionally, in the M-A-S-H xN y samples, the presence of sodium nitrate and/or the lower pH of the solution seems to slow down kinetic of formation of M-A-S-H phase compared to the pure M-S-H [32] and M-A-S-H [17] phases, but the temperature increase from 20 °C to 50 °C fasten the formation of M-A-S-H phases.

A similar complex mixture of different magnesium and aluminium containing solids can also be expected at the surface of cements exposed to seawater or at the interface with clays, where the presence of alkali sulphate, alkali carbonate and/or alkali chloride may influence the composition of the M-A-S-H phases by the formation of sulphate, carbonate and chloride hydrotalcite-like and zeolite-like phases. The further development of thermodynamic models for aluminium uptake in C-A-S-

H, M-A-S-H and hydrotalcite-like solids are very essential to describe changes at the interface of cement pastes with a magnesium containing environment or in cementitious materials based on magnesia-silica.

Declaration of Competing Interest

The authors declare that they have no known competing financial interests or personal relationships that could have appeared to influence the work reported in this paper.

Acknowledgements

The authors would like to thank Alexandre Dauzères and the French Institute of Radiation Protection and Nuclear Safety for the funding of Ellina Bernard's Ph.D.; Jorgen Skibsted is acknowledged for helpful discussion on the interpretation of NMR data. Céline Cau-Dit Coumes and Isabelle Pochard for the helpful discussions on the M-S-H and M-A-S-H structure, Rosa Guidone for the help with the samples handling. The NMR hardware was partially granted by the Swiss National Science Foundation (SNSF, grant no. 206021_150638/1).

Appendix A. Supplementary data

Supplementary data to this article can be found online at https://doi.org/10.1016/j.matdes.2020.109391.

References

[1] E. Gartner, T. Sui, Alternative cement clinkers, Cem. Concr. Res. 114 (2018) 27–39.
[2] S.A. Walling, J.L. Provis, Magnesia-based cements: a journey of 150 years, and cements for the future? Chem. Rev. 116 (2016) 4170–4204.
[3] J. Szczerba, R. Prorok, E. Śnieżek, D. Madej, K. Maślona, Influence of time and temperature on ageing and phases synthesis in the MgO–SiO_2–H_2O system, Thermochim. Acta 567 (2013) 57–64.
[4] C. Sonat, W. Teo, C. Unluer, Performance and microstructure of MgO-SiO_2 concrete under different environments, Constr. Build. Mater. 184 (2018) 549–564.
[5] A. Jenni, U. Mäder, C. Lerouge, S. Gaboreau, B. Schwyn, In situ interaction between different concretes and Opalinus clay, Phys. Chem. Earth, Parts A/B/C 70 (2014) 71–83.
[6] A. Dauzères, G. Achiedo, D. Nied, E. Bernard, S. Alahrache, B. Lothenbach, Magnesium perturbation in low-pH concretes placed in clayey environment - solid characterizations and modeling, Cem. Concr. Res. 79 (2016) 137–150.
[7] J.L. Garcia Calvo, A. Hidalgo, C. Alonso, L. Fernández Luco, Development of low-pH cementitious materials for HLRW repositories: resistance against ground waters aggression, Cem. Concr. Res. 40 (2010) 1290–1297.
[8] C. Lerouge, S. Gaboreau, S. Grangeon, F. Claret, F. Warmont, A. Jenni, V. Cloet, U. Mäder, In situ interactions between Opalinus clay and low alkali concrete, Physics and Chemistry of the Earth, Parts A/B/C 99 (2017) 3–21.
[9] U. Mäder, A. Jenni, C. Lerouge, S. Gaboreau, S. Miyoshi, Y. Kimura, V. Cloet, M. Fukaya, F. Claret, T. Otake, M. Shibata, B. Lothenbach, 5-year chemico-physical evolution of concrete-claystone interfaces, Swiss J. Geosci. 110 (2017) 307–327.
[10] D. Bonen, M.D. Cohen, Magnesium sulfate attack on Portland cement paste—II. Chemical and mineralogical analyses, Cem. Concr. Res. 22 (1992) 707–718.
[11] M. Santhanam, M.D. Cohen, J. Olek, Mechanism of sulfate attack: a fresh look: part 1: summary of experimental results, Cem. Concr. Res. 32 (2002) 915–921.
[12] K. De Weerdt, H. Justnes, The effect of sea water on the phase assemblage of hydrated cement paste, Cem. Concr. Compos. 55 (2015) 215–222.
[13] K. De Weerdt, B. Lothenbach, M. Geiker, Comparing chloride ingress from seawater and NaCl solution in Portland cement mortar, Cem. Concr. Res. 115 (2019) 80–89.
[14] D. Nied, K. Enemark-Rasmussen, E. L'Hopital, J. Skibsted, B. Lothenbach, Properties of magnesium silicate hydrates (MSH), Cem. Concr. Res. 79 (2016) 323–332.
[15] C. Roosz, S. Grangeon, P. Blanc, V. Montouillout, B. Lothenbach, P. Henocq, E. Giffaut, P. Vieillard, S. Gaboreau, Crystal structure of magnesium silicate hydrates (MSH): the relation with 2: 1 mg–Si phyllosilicates, Cem. Concr. Res. 73 (2015) 228–237.
[16] E. Bernard, B. Lothenbach, C. Chlique, M. Wyrzykowski, A. Dauzères, I. Pochard, C. Cau-Dit-Coumes, Characterization of magnesium silicate hydrate (M-S-H), Cem. Concr. Res. 116 (2019) 309–330.
[17] E. Bernard, B. Lothenbach, C. Cau-Dit-Coumes, I. Pochard, D. Rentsch, Aluminum incorporation into magnesium silicate hydrate (M-S-H), Cem. Concr. Res. 128 (2020) 105931.
[18] D. Madej, C. Ortmann, J. Szczerba, M. Jacewicz, Calorimetry and other methods in the studies of reactive magnesia–hydratable alumina–microsilica hydrating mixtures, J. Therm. Anal. Calorim. 126 (2016) 1133–1142.
[19] E. Bernard, B. Lothenbach, I. Pochard, C. Cau-Dit-Coumes, Alkali binding by magnesium silicate hydrates, J. Am. Ceram. Soc. 102 (2019) 6322–6336.
[20] E. Bernard, A. Jenni, M. Fisch, D. Grolimund, U. Mäder, Micro-X-ray diffraction and chemical mapping of aged interfaces between cement pastes and Opalinus Clay, Appl. Geochem. 115 (2020) 104538.
[21] T. Zhang, L.J. Vandeperre, C.R. Cheeseman, Formation of magnesium silicate hydrate (MSH) cement pastes using sodium hexametaphosphate, Cem. Concr. Res. 65 (2014) 8–14.
[22] M.B. Haha, B. Lothenbach, G. Le Saout, F. Winnefeld, Influence of slag chemistry on the hydration of alkali-activated blast-furnace slag—part I: effect of MgO, Cem. Concr. Res. 41 (2011) 955–963.
[23] A. Machner, M. Zajac, M.B. Haha, K.O. Kjellsen, M.R. Geiker, K. De Weerdt, Limitations of the hydrotalcite formation in Portland composite cement pastes containing dolomite and metakaolin, Cem. Concr. Res. 105 (2018) 1–17.
[24] S.A. Bernal, R. San Nicolas, R.J. Myers, R.M. de Gutiérrez, F. Puertas, J.S. van Deventer, J.L. Provis, MgO content of slag controls phase evolution and structural changes induced by accelerated carbonation in alkali-activated binders, Cem. Concr. Res. 57 (2014) 33–43.
[25] L. Vandeperre, M. Liska, A. Al-Tabbaa, Microstructures of reactive magnesia cement blends, Cem. Concr. Compos. 30 (2008) 706–714.
[26] S. Miyata, Anion-exchange properties of hydrotalcite-like compounds, Clay Clay Miner. 31 (1983) 305–311.
[27] P. Lalan, A. Dauzères, L. De Windt, D. Bartier, J. Sammaljärvi, J.-D. Barnichon, I. Techer, V. Detilleux, Impact of a 70° C temperature on an ordinary Portland cement paste/claystone interface: an in situ experiment, Cem. Concr. Res. 83 (2016) 164–178.
[28] B. Lothenbach, E. Bernard, U. Mäder, Zeolite formation in the presence of cement hydrates and albite, Phys. Chem. Earth, Parts A/B/C 99 (2017) 77–94.
[29] S.A. Walling, S.A. Bernal, L.J. Gardner, H. Kinoshita, J.L. Provis, Phase formation and evolution in mg $(OH)_2$–zeolite cements, Ind. Eng. Chem. Res. 57 (2018) 2105–2113.
[30] S.A. Bernal, J.L. Provis, V. Rose, R.M. De Gutierrez, Evolution of binder structure in sodium silicate-activated slag-metakaolin blends, Cem. Concr. Compos. 33 (2011) 46–54.
[31] S.A. Bernal, J.L. Provis, R.J. Myers, R. San Nicolas, J.S. van Deventer, Role of carbonates in the chemical evolution of sodium carbonate-activated slag binders, Mater. Struct. 48 (2015) 517–529.
[32] E. Bernard, B. Lothenbach, D. Rentsch, I. Pochard, A. Dauzères, Formation of magnesium silicate hydrates (M-S-H), Phys. Chem. Earth, Parts A/B/C 99 (2017) 142–157.
[33] E. L'Hôpital, B. Lothenbach, G. Le Saout, D. Kulik, K. Scrivener, Incorporation of aluminium in calcium-silicate-hydrates, Cem. Concr. Res. 75 (2015) 91–103.
[34] D. Massiot, F. Fayon, M. Capron, I. King, S. Le Calvé, B. Alonso, J.O. Durand, B. Bujoli, Z. Gan, G. Hoatson, Modelling one-and two-dimensional solid-state NMR spectra, Magn. Reson. Chem. 40 (2002) 70–76.
[35] R.K. Harris, E.D. Becker, S.M.C. De Menezes, R. Goodfellow, P. Granger, NMR nomenclature. Nuclear spin properties and conventions for chemical shifts (IUPAC recommendations 2001), Pure Appl. Chem. 73 (2001) 1795–1818.
[36] A. Kentgens, A practical guide to solid-state NMR of half-integer quadrupolar nuclei with some applications to disordered systems, Geoderma 80 (1997) 271–306.
[37] D. Kulik, T. Wagner, S.V. Dmytrieva, G. Kosakowski, F. Hingerl, K.V. Chudnenko, U. Berner, GEM-Selektor geochemical modeling package: revised algorithm and GEMS3K numerical kernel for coupled simulation codes, Computational Geochemistry 17 (2013) 1–24.
[38] T. Thoenen, W. Hummel, U. Berner, E. Curti, The PSI/Nagra Chemical Thermodynamic Database 12/07, PSI Report 14–04, Villigen PSI, Switzerland, 2014.
[39] E. Bernard, B. Lothenbach, C. Cau-Dit-Coumes, C. Chlique, A. Dauzères, I. Pochard, Magnesium and calcium silicate hydrates, part I: investigation of the possible magnesium incorporation in calcium silicate hydrate (C-S-H) and of the calcium in magnesium silicate hydrate (M-S-H), Appl. Geochem. 89 (2018) 229–242.
[40] B. Lothenbach, L. Pelletier-Chaignat, F. Winnefeld, Stability in the system CaO–Al_2O_3–H_2O, Cem. Concr. Res. 42 (2012) 1621–1634.
[41] B. Lothenbach, D.A. Kulik, T. Matschei, M. Balonis, L. Baquerizo, B. Dilnesa, G.D. Miron, R.J. Myers, Cemdata18: a chemical thermodynamic database for hydrated Portland cements and alkali-activated materials, Cem. Concr. Res. 115 (2019) 472–506.
[42] B. Lothenbach, F. Winnefeld, Thermodynamic modelling of the hydration of Portland cement, Cem. Concr. Res. 36 (2006) 209–226.
[43] B. Ma, B. Lothenbach, Synthesis, characterization, and thermodynamic study of selected Na-based zeolites, Cem. Concr. Res. 135 (2020) 106111.
[44] B. Lothenbach, P. Durdzinski, K. DeWeerdt, Thermogravimetric analysis, in: K. Scrivener, R. Snellings, B. Lothenbach (Eds.), A Practical Guide to Microstructural Analysis of Cementitious Materials, CRC Press, Oxford, UK 2016, pp. 177–212.
[45] F. Jin, A. Al-Tabbaa, Thermogravimetric study on the hydration of reactive magnesia and silica mixture at room temperature, Thermochim. Acta 566 (2013) 162–168.
[46] T. Zhang, J. Zou, B. Wang, Z. Wu, Y. Jia, C.R. Cheeseman, Characterization of magnesium silicate hydrate (MSH) gel formed by reacting MgO and silica fume, Materials 11 (2018) 909.
[47] D.R.M. Brew, F.P. Glasser, Synthesis and characterisation of magnesium silicate hydrate gels, Cem. Concr. Res. 35 (2005) 85–98.
[48] T. Zhang, C. Cheeseman, L. Vandeperre, Development of low pH cement systems forming magnesium silicate hydrate (MSH), Cem. Concr. Res. 41 (2011) 439–442.
[49] J. Katanić-Popović, N. Miljević, S. Zec, Spinal formation from coprecipitated gel, Ceram. Int. 17 (1991) 49–52.
[50] D. Madej, Examination of dehydration and dehydroxylation of synthetic layered (oxy) hydroxides through thermal analysis (TG-DSC-EGA-MS) and a discussion to the second Pauling's rule, Inorg. Chim. Acta 482 (2018) 402–410.
[51] A. Cuesta, R.U. Ichikawa, D. Londono-Zuluaga, G. Angeles, I. Santacruz, X. Turrillas, M.A. Aranda, Aluminum hydroxide gel characterization within a calcium aluminate cement paste by combined pair distribution function and Rietveld analyses, Cem. Concr. Res. 96 (2017) 1–12.

[52] T. Isobe, T. Watanabe, J.-B.d.E.d. Lacaillerie, A. Legrand, D. Massiot, Solid-state ^{1}H and ^{27}Al NMR studies of amorphous aluminum hydroxides, Journal of colloid and interface science, 261 (2003) 320–324.
[53] I. Hassan, H.D. Grundy, Structure of basic sodalite, $Na_8Al_6Si_6O_{24}(OH)_2.2H_2O$, Acta Crystallographica C39 (1983) 3–5.
[54] G. Gottardi, E. Galli, Natural Zeolites Springer-Verlag, Berlin-Heidelberg, Germany, 1985.
[55] J.-B. d'Espinose de Lacaillerie, M. Kermarec, O. Clause, ^{29}Si NMR observation of an amorphous magnesium silicate formed during impregnation of silica with mg(II) in aqueous solution, J. Phys. Chem. 99 (47) (1995) 17273–17281.
[56] J.S. Hartman, R.L. Millard, Gel synthesis of magnesium silicates: a ^{29}Si magic angle spinning NMR study, Phys. Chem. Miner. 17 (1990) 1–8.
[57] J. Temuujin, K. Okada, K.J. MacKenzie, Formation of layered magnesium silicate during the aging of magnesium hydroxide–silica mixtures, J. Am. Ceram. Soc. 81 (1998) 754–756.
[58] S.A. Walling, H. Kinoshita, S.A. Bernal, N.C. Collier, J.L. Provis, Structure and properties of binder gels formed in the system $mg(OH)_2$-SiO_2-H_2O for immobilisation of Magnox sludge, Dalton Trans. 44 (2015) 8126–8137.
[59] M. Tonelli, F. Martini, L. Calucci, E. Fratini, M. Geppi, F. Ridi, S. Borsacchi, P. Baglioni, Structural characterization of magnesium silicate hydrate: towards the design of eco-sustainable cements, Dalton Trans. 45 (2016) 3294–3304.
[60] P.S. Neuhoff, S. Kroeker, L.-S. Du, T. Fridriksson, J.F. Stebbins, Order/disorder in natrolite group zeolites: a ^{29}Si and ^{27}Al MAS NMR study, Am. Mineral. 87 (2002) 1307–1320.
[61] E. Lippmaa, M. Maegi, A. Samoson, M. Tarmak, G. Engelhardt, Investigation of the structure of zeolites by solid-state high-resolution silicon-29 NMR spectroscopy, J. Am. Chem. Soc. 103 (1981) 4992–4996.
[62] K.J. MacKenzie, R.H. Meinhold, B.L. Sherriff, Z. Xu, ^{27} Al and ^{25} mg solid-state magic-angle spinning nuclear magnetic resonance study of hydrotalcite and its thermal decomposition sequence, J. Mater. Chem. 3 (1993) 1263–1269.
[63] E. Lippmaa, A. Samoson, M. Magi, High-resolution aluminum-^{27} NMR of aluminosilicates, J. Am. Chem. Soc. 108 (1986) 1730–1735.
[64] J. Klinowski, Nuclear magnetic resonance studies of zeolites, Prog. Nucl. Magn. Reson. Spectrosc. 16 (1984) 237–309.
[65] T. Hibino, A. Tsunashima, Characterization of repeatedly reconstructed mg— Al hydrotalcite-like compounds: gradual segregation of aluminum from the structure, Chem. Mater. 10 (1998) 4055–4061.
[66] J. Sanz, J. Serratosa, Silicon-29 and aluminum-27 high-resolution MAS-NMR spectra of phyllosilicates, J. Am. Chem. Soc. 106 (1984) 4790–4793.
[67] K.J. MacKenzie, R.H. Meinhold, A.K. Chakravorty, M. Dafadar, Thermal reactions of alkali-leached aluminosilicates studied by XRD and solid-state 27 Al, 29 Si and 23 Na MAS NMR, J. Mater. Chem. 6 (1996) 833–841.
[68] P. Duxson, G. Lukey, F. Separovic, J. Van Deventer, Effect of alkali cations on aluminum incorporation in geopolymeric gels, Ind. Eng. Chem. Res. 44 (2005) 832–839.
[69] I. García-Lodeiro, A. Fernández-Jiménez, A. Palomo, D.E. Macphee, Effect of calcium additions on N–A–S–H cementitious gels, J. Am. Ceram. Soc. 93 (2010) 1934–1940.
[70] H. Yang, R.I. Walton, S. Antonijevic, S. Wimperis, A.C. Hannon, Local order of amorphous zeolite precursors from ^{29}Si {H} CPMAS and ^{27}Al and ^{23}Na MQMAS NMR and evidence for the nature of medium-range order from neutron diffraction, J. Phys. Chem. B 108 (2004) 8208–8217.
[71] S.K. Lee, J.F. Stebbins, The distribution of sodium ions in aluminosilicate glasses: a high-field Na-23 MAS and 3Q MAS NMR study, Geochim. Cosmochim. Acta 67 (2003) 1699–1709.
[72] E. Bernard, B. Lothenbach, F. Le Goff, I. Pochard, A. Dauzères, Effect of magnesium on calcium silicate hydrate (C-S-H), Cem. Concr. Res. 97 (2017) 61–72.
[73] E. L'Hôpital, B. Lothenbach, K. Scrivener, D. Kulik, Alkali uptake in calcium alumina silicate hydrate (CASH), Cem. Concr. Res. 85 (2016) 122–136.
[74] K. Rozov, U. Berner, C. Taviot-Gueho, F. Leroux, G. Renaudin, D. Kulik, L.W. Diamond, Synthesis and characterization of the LDH hydrotalcite–pyroaurite solid-solution series, Cem. Concr. Res. 40 (2010) 1248–1254.
[75] M. Vespa, C. Borca, T. Huthwelker, B. Lothenbach, R. Dähn, E. Wieland, Structural characterisation of magnesium (sodium) Aluminium silicate hydrate (M-(N)-A-S-H) phases by X-ray absorption near-edge spectroscopy, Appl. Geochem. 104750 (2020).